ORIGINAL STUDY

Numerical study on the effects of fracture parameters on permeability in fractured rock with extremely low matrix permeability

Guiwu Chen[1] · Lei Song[1] · Wenliang Zhang[1]

© Akadémiai Kiadó 2021

Abstract
Understanding the permeability of fractured rocks can make for significant advances in the development of fluid flow and mass transport modeling. This paper investigates the effects of fracture number, length, and aperture on the permeability of fractured rocks with extremely low matrix permeability. For this purpose, we apply numerical estimations of fracture-scale permeability to fractured rock samples containing 3D discrete fracture networks (DFNs). The resulting permeability behavior is analyzed for the number, the aperture and the length distribution of the fractures. Our results indicate that permeability is sensitive not only to the fracture number but also to the geometrical characteristics of DFN. In particular, our study suggests that the increase in fractures parameters increases the uncertainty of the relation between fracture parameters and permeability. The comparison of permeability values with fractures intersections shows that increasing permeability coincides with increasing intersection points number and a total length of intersection lines.

Keywords Permeability estimation · Fluid flow modeling · Stochastic fracture networks

1 Introduction

Permeability in natural fractured rocks is important as it has a major effect on fluid flow. In geothermal projects (Hanano 2004; Nathenson 2000; Slatlem Vik et al. 2018) it is extremely vital to study permeability of fractured medium for modeling of heat flow in heat chambers. It is also of great importance in oil and gas industry (Tayari et al. 2018; Wei et al. 2018) where permeability strongly controls the oil and gas translation and extraction. Another important application is in water reservoirs (Hunt 2005; Wang and Park 2002) the

---

✉ Lei Song
songlei@cumt.edu.cn

Guiwu Chen
guiwu_chen@cumt.edu.cn

Wenliang Zhang
wenliangzhang@cumt.edu.cn

[1] State Key Laboratory for Geomechanics and Deep Underground Engineering, China University of Mining and Technology, Xuzhou 221116, China

extent and the quality of an aquifer is directly affected by the permeability of the host and surrounding rocks.

Geophysical methods can be an effective nondestructive technique for permeability prediction of a formation (Fabricius et al. 2007; Fang et al. 2018). However, permeability cannot be linked to geophysical responses (such as logging and seismic data) directly and is often indirectly derived from porosity values computed from acoustic impedances. Therefore, understanding the fluid flow of fractured rocks is of great importance for geophysical methods for permeability estimation, which prompted intensive studies of realistic modeling of fractures. Fractures are typically conceptualized as objects with high fluid permeability and high mechanical compressibility (Xu and Yu 2008; Narsilio et al. 2009; Mostaghimi et al. 2013). For reservoirs with extremely low matrix permeability, fracture networks predominant pathways for the migration of fluids (Roy 2019; Szabó et al. 2015). However, the inherent structural randomness of most fractured rocks can result in a complex hydraulic heterogeneity. Therefore, accurate representations of the fractures and efficient evaluation of their influences on permeability are very important for investigation of the fluid flow in fractured rock masses. Although, linking measured large scale permeability directly to exact fracture parameters is difficult, since the fracture sizes are generally much smaller than the scale of Representative Elemental Volume (REV), acquiring an effective value of fractured rocks in REV can be realized. The effective medium approximations and the Kozeny-Carman relationships have been developed for permeability estimation from internal structure information (Xu and Yu 2008). It has been demonstrated that the simple objects, such as the regularly distributed rectangles or ellipsoids, can be reliably estimated but the complicated rock structures remain enigmatic (Mostaghimi et al. 2013; Narsilio et al. 2009). To improve modelling accuracy, there is an urgent need to develop an integrated method for combination of stochastic fracture networks methods and micro-scale fluid flow modelling approaches. Concerning fractured rocks, the ensemble flow response can be quantified by block or equivalent permeability (Amaziane et al. 2001). The flow paths of fractured rocks are mainly controlled by connected fractures, and the hydraulic response of fracture network is of particular importance for characterizing the large scale fluid flow (Huang et al. 2017). In addition, natural fractured rocks usually display a strong hydraulic complexity causing by the internal morphology of fractures (Li et al. 2016; Zhang et al. 2014) and from their distributions in rocks. (Zhang and Yin 2014). (de Dreuzy et al. 2001a, b) conducted numerical tests of water flow through 2D random fracture networks to study the influence of effective connectivity and aperture on hydraulic properties. The 3D DFNs are advantageous to describe the real fracture parameters, such as orientation, connectivity and location, and giving a more reliable permeability result. In recent research, 3D DFNs were used to study how the surface roughness and connectivity of fracture network can affect the nonlinear flow regimes (Xiong et al. 2019). Further progress in fluid flow and mass transport modeling of natural fracture networks, however, requires a better understanding of the relationship between the fracture parameters and permeability. This paper will focus on developing a workflow for estimation of absolute permeability in discrete fracture network rocks using the Darcian continuum theory and single-phase flow velocity in 3D fractured rocks.

Several direct simulation methods are widely used to model fluid flow within heterogeneous fracture spaces (Khirevich et al. 2015; Starnoni et al. 2017). In direct simulations, the governing equations are solved on the real fracture-space of rocks. Finite difference method (FDM) is another popular direct approach allowing for solving the Navier–Stokes equations directly on 3D images. As noted previously, all computational methods have high computational costs when applied to three-dimensional problems. To

improve computational efficiency, (Gerke et al. 2018) developed smart and parallel computing software based on FDM scheme to obtain fluid flow velocity and pressure field within heterogeneous medium.

Although many researches have been conducted on fluid flow, studies on the impact of stochastic features of fracture parameters on permeability prediction remains largely unexplored. In this paper, the effects of stochastic properties of fracture networks on absolute permeability are investigated by integrating 3D DFNs generating, fluid flow modeling and permeability calculating. Fluid flow modeling in our study was carried out by solving the Navier–Stokes equations directly using FDM on 3D models with different fracture parameters. Finally, the absolute permeability results and uncertainty analysis for the relationship between permeability and fracture parameters are presented.

2 Fracture model

The geometrical constitution of the natural fracture systems can be described as a set of convex polygons. The shapes, sizes and locations of these polygons are random. Based on this assumption, fractures were represented as a set of 3D irregular convex polygons, and their sizes followed the negative exponential distribution function (Cheng-Haw et al. 2006; Zazoun 2008). The probability density function PDF $f_X(x)$ of a negative exponential distribution Exp (λ) with mean $\mu_X = \lambda$ and variance $\sigma_X = \lambda^2$ can be obtained as follow (Grana et al. 2014):

$$f_X(x) = \begin{cases} \frac{1}{\lambda}e^{-\frac{x}{\lambda}}, x > 0, \\ 0, x \leq 0. \end{cases} \tag{1}$$

where $\lambda > 0$. Their locations were determined by means of three dimensional uniform distributions discretely. A fracture plane orientation is given by two angles, dip and strike (or dip direction), see Fig. 1 for details. Fracture orientation is determined by the direction of the fracture, dip angle and strike angle. The intersection line between the fracture and the horizontal plane is OA, and the angle between OA and the Y-axis is the strike angle, which indicates the extension direction of the fracture. OB is a straight line on the fracture and perpendicular to OA, OC is the projection of OB on the horizontal plane, and the angle between OB and OC is dip angle, which shows the inclination degree of fracture. Strike and dip angles were obtained from uniform and Fisher distributions, respectively. For a single fracture, the mean dip angle was π/4 and its variation was π/8. The mean strike angle was π and variation was π/4. For a fracture network, the region of study is a cube bounded by [x_{min}, x_{max}, y_{min}, y_{max}, z_{min}, z_{max}], DFN can be built directly using ADFNE package, see (Fadakar Alghalandis 2017) for more details about 3D DFNs construction.

The samples were set to a cube with a side length (L) of 300 μm. To guarantee the integrity of fractured samples, the maximum length value of fractures equaled to $l_{max} = L/2 = 150$ μm.

The fracture numbers n were varied from 100 to 500 and consider four mean values of the fracture length (μ) distribution: $\mu/L = 0.25$, $\mu/L = 0.30$, $\mu/L = 0.35$ and $\mu/L = 0.40$. For each combination of the fracture parameters, containing fracture number n, the mean fracture length μ and aperture δ, we generated a DFN. Figure 2 shows 20 realizations of 3D DFNs with different combinations of fracture number and average length value to demonstrate the internal structures of fracture networks. The fracture number n and the ratio μ/L are increased from top to bottom and from left to right, respectively. With respect to a
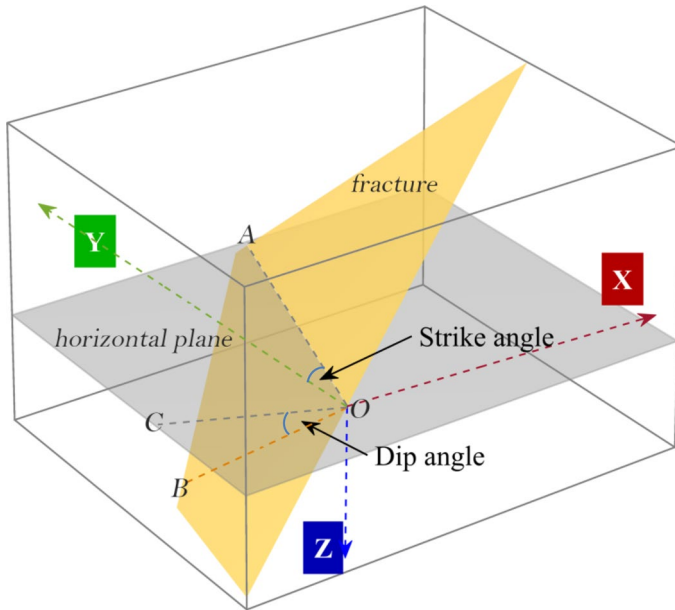
Fig. 1 The fracture orientation parameters in 3D

smaller μ/L, smaller fractures dominate the network structure. As μ/L increases, the variance σ increases as well, the relative number of smaller fractures decreases. Increasing the parameter n increases fracture density.

3 Numerical estimation of permeability in discrete fracture network rocks

To study the permeability of Darcian flow for the considered fractured rock sample, we perform single-phase fracture-scale flow tests. In Cartesian coordinate system (x, y, z), let velocity vector $\boldsymbol{v}$ (v_x, v_y, v_z) and pressure field $\boldsymbol{p}$ (p_x, p_y, p_z) be function of x, y and z. To this end, we solve the Stokes equation (Gerke et al. 2018) formulated for flow velocity field $\boldsymbol{v}$ and pressure field $\boldsymbol{p}$ in 3D space domain.

$$\begin{cases} \mu \Delta \boldsymbol{v} - \nabla \mathbf{p} = 0 \\ div \boldsymbol{v} = 0 \end{cases} \tag{2}$$

under the assumption that Reynolds number (Re) is small:

$$\mathrm{Re} = \frac{\rho v l}{\mu}, \; Re << 1 \tag{3}$$

where μ and ρ are the viscosity and density of fluid.

We solved Eq. (2) numerically using the FDMSS open source software (Gerke et al. 2018) to obtain a velocity field under the pressure boundary conditions decided by $\Delta p/L = \mathrm{grad} p = 1$. According to Darcy's law, the permeability of a given rock sample can be computed as
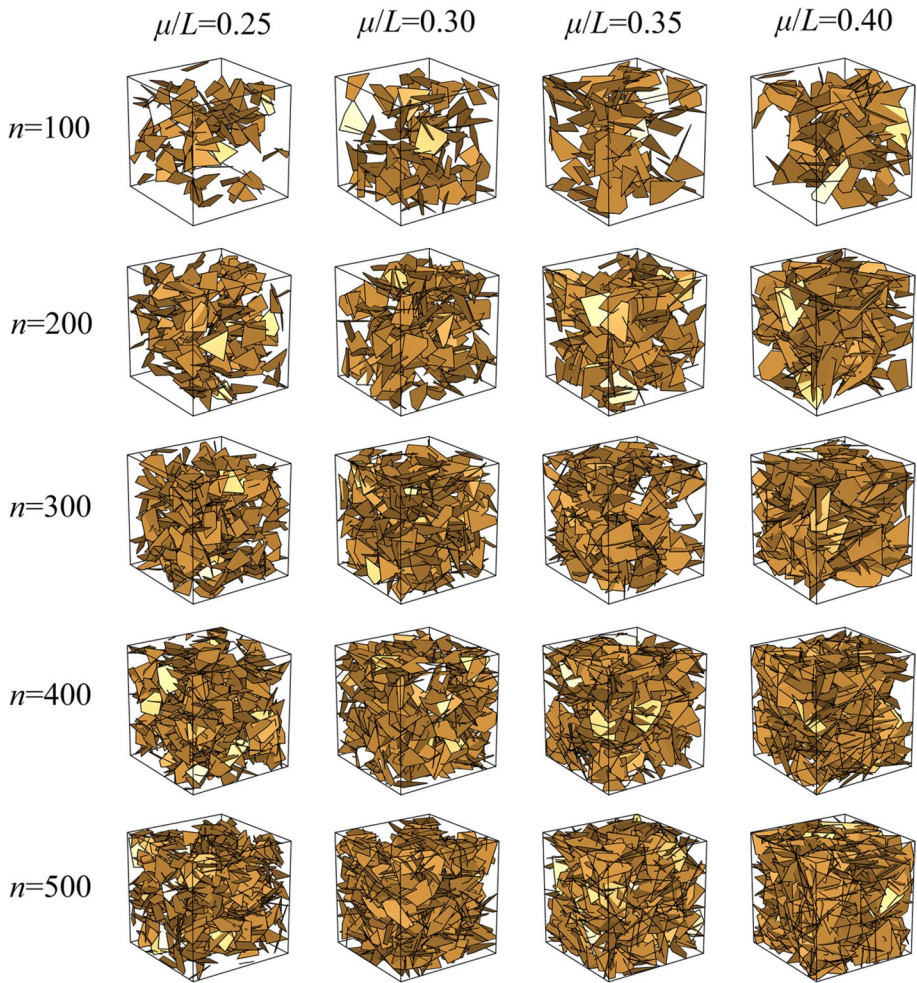
Fig. 2 3D DFN models with different fracture numbers and length distributions. The corresponding values of the fracture mean length μ and the fracture numbers n are given in the plot

$$K = \frac{\mu L Q}{\Delta p S} = \frac{\mu Q}{S} \tag{4}$$

where K is permeability, Δp is the pressure difference generated by the distance L. Consider a cross-sectional area S, the effective area (pores area) and the average velocity over the whole cross-sectional area are S_{eff} and v_{eff} respectively, then flow rate Q through it can be computed according to:

$$Q = v_{eff} S_{eff} \tag{5}$$

So the permeability can be calculated as

$$K = \frac{\mu \nu_{eff} S_{eff}}{S} \qquad (6)$$

In practice, the ratio of effective porosity V_{fracture} to the volume V is more accurate than S_{eff} to the areas S, we obtain

$$K = \frac{\mu \langle \nu \rangle V_{fracture}}{V} \qquad (7)$$

Above, the flowchart to determine the permeability of a rock sample containing DFN can be summarized in Fig. 3. The steps are:

1. Input fracture parameters: fracture number, mean length and aperture;
2. Using the ADFNE package (Fadakar Alghalandis 2017) to create 3D DFN;
3. Transform DFN to 3D image;
4. Solving the Stokes equation directly on the voxelized 3D images to obtain flow velocity using the FDMSS software;
5. Substitute the average flow velocity into the Darcian equation to calculate the scalar values of permeability.

4 Results and discussion

To investigate the influences of length distribution, fracture number and aperture on absolute permeability, we conduct the following numerical experiments. For all the calculations, pressures at every pixel were assigned according to $\Delta p/L = \mathrm{grad}\, p = 1$ kg/(vx$^2 \times$s^2), and μ was fixed to 100 kg/(vx$\times$s), where vx refers to the voxel size. We consider five different values of n, four different values of μ and four different apertures, and obtained 80 different models. The side length L was fixed at 300 μm. Our numerical models were transformed to $301 \times 301 \times 301$ discretized 3D images with an even spatial spacing of 1 μm. In our 3D image files, 0 and 1 represent fractures and solids respectively. The computation results of permeability are given in Table 1. Three numbers of model names represent fracture number, mean length, and aperture, respectively. For example, 300_0.25–1 indicates the computation results of the fracture model with 300 fractures, the ratio of fracture mean length and sample length μ/L and aperture δ equal to 0.25 and 1 μm respectively.

4.1 Permeability as a function of fracture number n

In the first section, the fracture aperture and mean length were fixed to a certain value ($\mu/L = 0.35$ and $\delta = 3$ μm), and fracture number was changed from 100 to 500 to explore how fracture number can affect the permeability of fractured rocks. Figure 4 shows the Darcian permeability as a function of fracture number in the range of 100 to 500 for four different combinations of fracture mean length and aperture. From Fig. 4, the permeability changes hardly with the increase of fracture number when $\mu/L = 0.25$, $\delta = 1$ μm. With μ/L increase to 0.35 and δ keep to 1 μm, it can be found that the permeability also remain almost constant. However, when δ increase to 3 μm, $\mu/L = 0.25$, the permeability is positive correlated with the fracture number. Especially for $\mu/L = 0.35$, the permeability rising tendency remarkably increase with the increase of the fracture number. Hence,
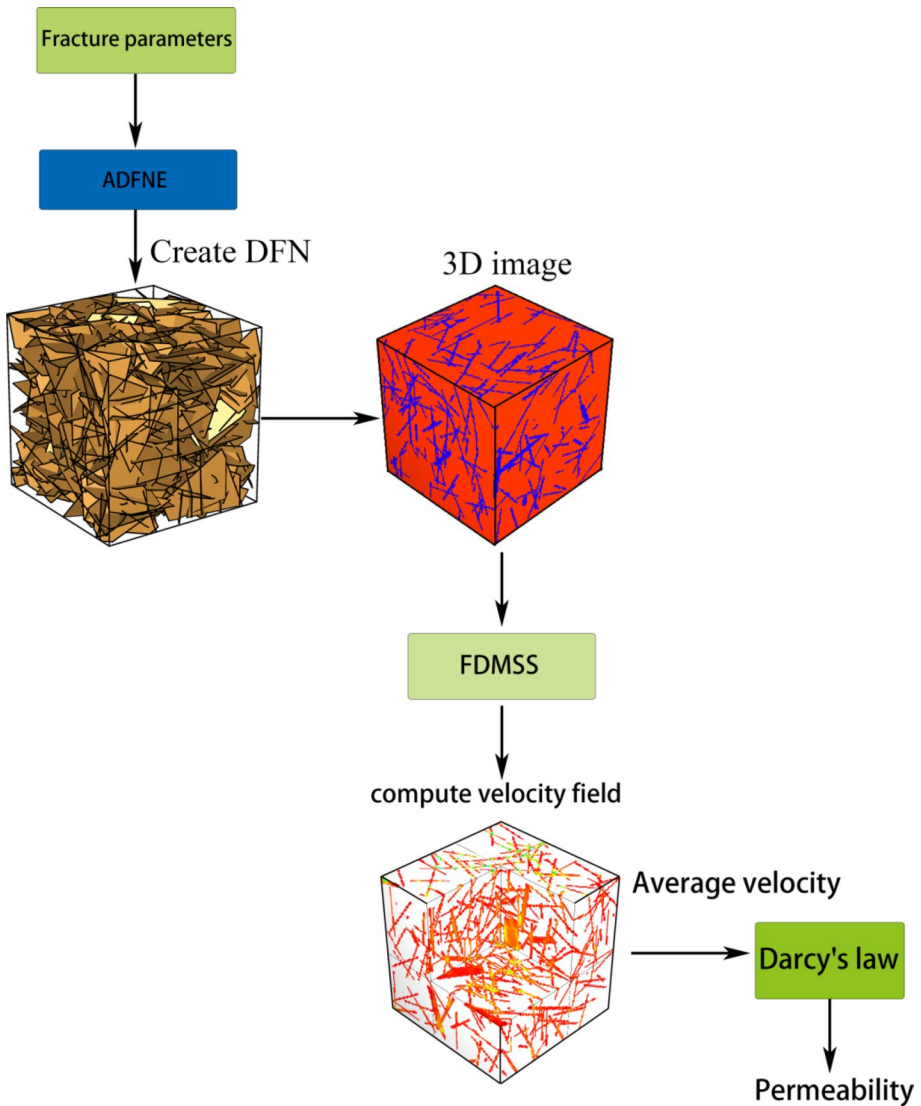
Fig. 3 Workflow for permeability estimation in a rock sample containing 3D DFN

on the one hand, it is indicated that the lower level of δ results in the lower permeability in the fracture number range of the 100–500, and for a rock with low fracture aperture the increment of μ/L has subtle influence on the relationship between permeability and the fracture number. The higher δ enhances the positive influence of μ/L on the rising tendency of permeability with the increase of fracture number. On the other hand, the increment of δ reinforces the positive relationship between the permeability and the fracture number a little on the condition of lower μ/L value 0.25. With the larger μ/L

Table 1 Permeability results of 80 different fracture parameter combinations

Fracture model	Permeability (mD)	Fracture model	Permeability (mD)	Fracture model	Permeability (mD)	Fracture model	Permeability (mD)
100_0.25–1	0.0106718	100_0.30–1	0.0253759	100_0.35–1	0.0635987	100_0.40–1	0.098933
100_0.25–2	0.0513892	100_0.30–2	0.184133	100_0.35–2	0.447709	100_0.40–2	0.681583
100_0.25–3	0.0739064	100_0.30–3	0.677313	100_0.35–3	1.69597	100_0.40–3	2.69313
100_0.25–4	0.106232	100_0.30–4	1.51332	100_0.35–4	5.12403	100_0.40–4	7.70591
200_0.25–1	0.0477826	200_0.30–1	0.0977004	200_0.35–1	0.302536	200_0.40–1	0.506882
200_0.25–2	0.233419	200_0.30–2	0.852276	200_0.35–2	3.28208	200_0.40–2	5.32833
200_0.25–3	0.642891	200_0.30–3	2.99244	200_0.35–3	12.411	200_0.40–3	20.4285
200_0.25–4	2.32941	200_0.30–4	9.27803	200_0.35–4	32.9864	200_0.40–4	56.6245
300_0.25–1	0.115065	300_0.30–1	0.272251	300_0.35–1	0.757885	300_0.40–1	1.26186
300_0.25–2	1.13617	300_0.30–2	3.23607	300_0.35–2	8.22411	300_0.40–2	13.1776
300_0.25–3	4.4661	300_0.30–3	13.2927	300_0.35–3	31.6191	300_0.40–3	50.0618
300_0.25–4	12.9944	300_0.30–4	36.5993	300_0.35–4	86.1538	300_0.40–4	136.881
400_0.25–1	0.177677	400_0.30–1	0.412301	400_0.35–1	1.04922	400_0.40–1	1.83252
400_0.25–2	2.05369	400_0.30–2	5.48609	400_0.35–2	12.5743	400_0.40–2	18.4788
400_0.25–3	8.63047	400_0.30–3	23.7641	400_0.35–3	50.4011	400_0.40–3	72.2123
400_0.25–4	26.1014	400_0.30–4	68.9387	400_0.35–4	141.065	400_0.40–4	200.816
500_0.25–1	0.298483	500_0.30–1	0.851473	500_0.35–1	1.42456	500_0.40–1	2.63018
500_0.25–2	3.42957	500_0.30–2	10.2486	500_0.35–2	17.479	500_0.40–2	25.8172
500_0.25–3	15.3847	500_0.30–3	42.0896	500_0.35–3	70.2019	500_0.40–3	100.145
500_0.25–4	44.8962	500_0.30–4	118.148	500_0.35–4	198.474	500_0.40–4	326.131

Fig. 4 Validation and comparison of Darcian permeability as a function of fracture number for four different combinations of fracture mean length and aperture
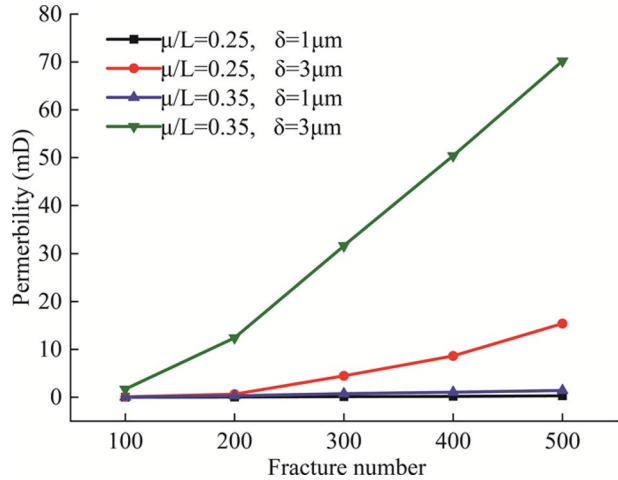

value 0.35, the slope of the relationship between the permeability and the fracture number increases when the δ value increases.

4.2 Permeability as a function of fracture length distribution

In the second section, the fracture number and aperture were fixed to a certain value ($n=400$ and $\delta=3$ μm), and the ratio of facture mean length and sample length μ/L was changed from 0.25 to 0.40 to explore how fracture mean length can affect the permeability of fractured rocks. Figure 5 represents the Darcian permeability as a function of the ratio μ/L for four different combinations of fracture number and aperture. The permeability keeps a small value (approaching 0) despite the μ/L increases from 0.25 to 0.4 on the condition of $\delta=1$ μm. Once $n=400$, $\mu/L=0.25$, the permeability increases slowly with the increase of fracture aperture. The rising tendency of the permeability is more obvious

Fig. 5 Validation and comparison of Darcian permeability as a function of fracture mean length for four different combinations of fracture number and aperture
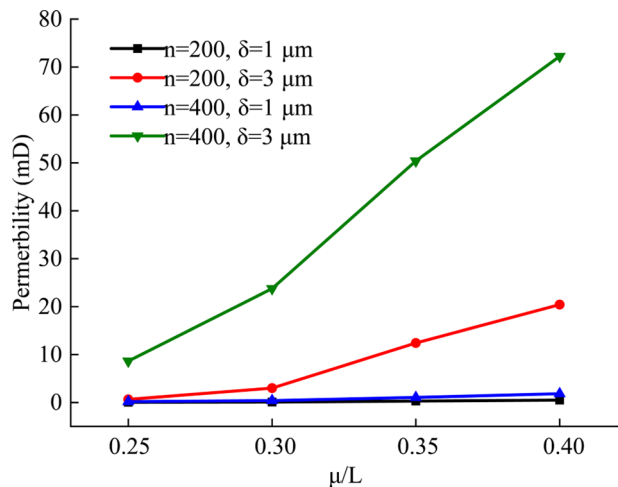
when $n = 200$, $\mu/L = 0.35$. It is indicated that μ/L has more importance on the permeability than the fracture number. While, on the condition of $\mu/L = 0.35$, the increased fracture number 400 enlarge the increasing tendency of permeability apparently.

4.3 Permeability as a function of fracture aperture

In the third section, keeping the fracture number and mean length to a certain value ($n = 400$ and $\mu/L = 0.35$), and changing the fracture aperture δ from 1 to 4 µm to explore how fracture aperture can affect the permeability of fractured rocks. Figure 6 shows the Darcian permeability as a function of the aperture in the range of 1 to 4 µm for four different combinations of fracture mean length and number. From Fig. 6, the permeability changes hardly with the increase of fracture number when $n = 200$, $\mu/L = 0.25$. With n increase to 400 and μ/L keep to 0.25, it can be found that the permeability increases slowly with the increase of fracture aperture. However, when μ/L increase to 0.35, $n = 200$, the permeability is positive correlated with the fracture aperture. Especially for $n = 400$, the permeability rising tendency remarkably increase with the increase of the fracture aperture.

4.4 Multivariate regression analysis of fracture parameters and permeability

We increased numerical realizations for each parameter combination to 5.400 results were obtained, and a multivariate regression of the data of fracture number, mean length, aperture and permeability using

$$
\begin{aligned}
Permeability = {}& 353.6333 - 160.8944 \cdot \delta - 850.2991 \cdot (\mu/L) \\
& + 277.8966 \cdot (\mu/L) \cdot \delta - 0.6937293 \cdot n + 0.1358125 \cdot n \cdot \delta \\
& + 1.551118 \cdot n \cdot (\mu/L) + 10.86022 \cdot \delta^2
\end{aligned}
\tag{8}
$$

fits the data quite well. The result clearly shows that in the formation with extremely low matrix permeability, the permeability increases almost linearly with fracture number and length while quadratically with aperture.

Fig. 6 Validation and comparison of Darcian permeability as a function of aperture for four different combinations of fracture number and mean length
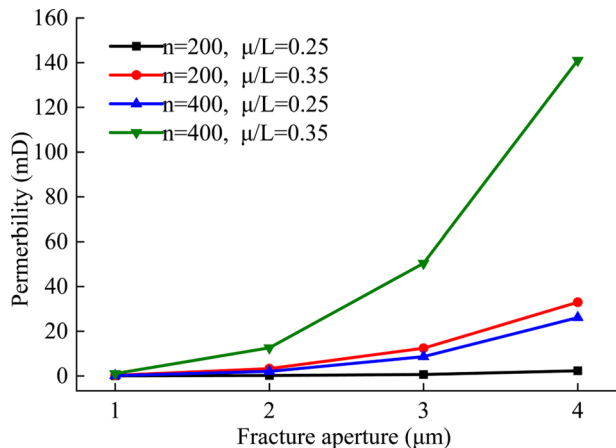
4.5 Intersection analysis

In fractured rocks, fracture connectivity controls fluid flow. The intersections between fractures are the key indicator for describing the fracture connectivity in fractured rocks (Dong et al. 2018). Planar polygons were used for fracture representations and therefore the length of fracture intersection becomes the length of the line of intersection between planar polygons in 3D (see Fig. 7). The number of intersections and the total length of intersection lines refer to the number and the total length of the lines of intersections in a DFN models, respectively.

The range of considered fracture distribution parameters μ and n are closely related to fracture connectivity. In order to facilitate the interpretation of the permeability of the four types of fracture length distributions ($\mu/L=0.25$, $\mu/L=0.30$, $\mu/L=0.35$ and $\mu/L=0.40$) and three fracture numbers ($n=300$, $n=400$ and $n=500$) considered from the perspective of fracture connectivity, we compared the permeability values for each individual fracture network at a given aperture ($\delta=3$ μm). For each parameter combination, 5 realizations were conducted. The number and the total length of intersection lines of each fracture network as well as the permeability are plotted in Fig. 8a and b, respectively.

Permeability exhibits an overall increase with an increase in fracture intersection number and total length of intersection lines. The presence of more fracture connectivity increases the fluid flow and, therefore, uppers the permeability. Robust regression was used to compute the fit lines. The correlation coefficients of fitted lines on Fig. 8 a, b are 0.9842 and 0.9940, respectively. Thus, permeability shows a closer link with total length of intersection lines than the intersection number. Figure 8 also presents the variability of permeability is increasing with increasing n and μ. Thus, the larger fracture parameters combination has a larger uncertainty of permeability prediction.
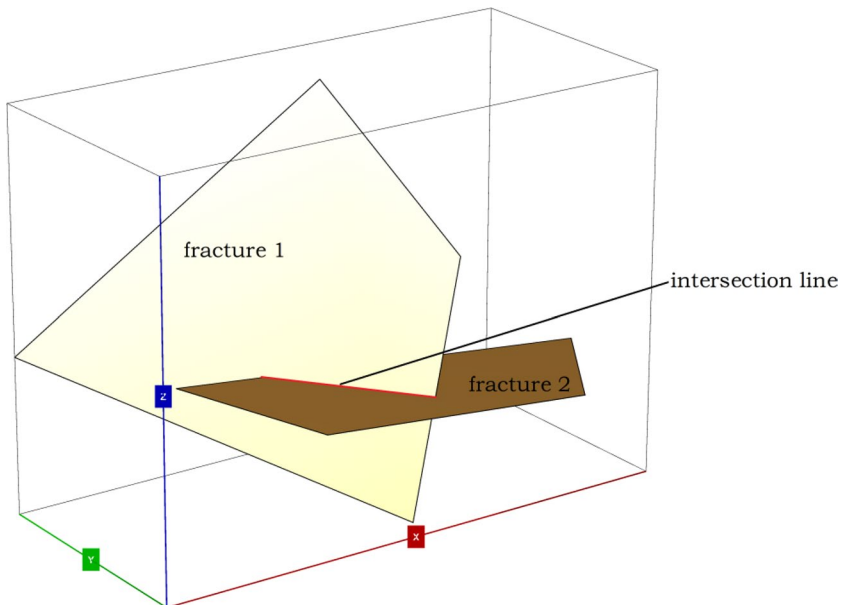

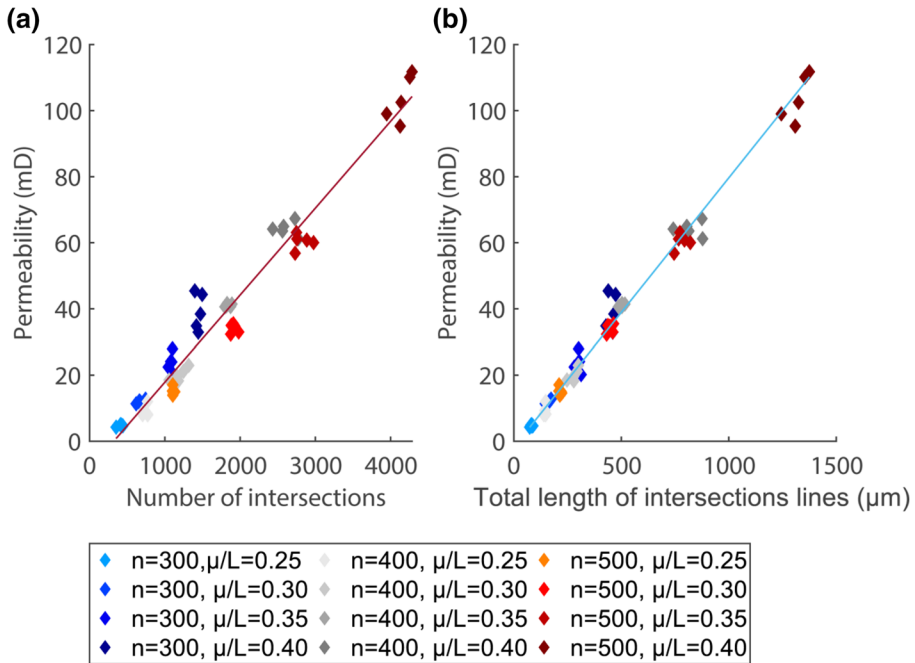**Fig. 7** Intersection between two fractures in 3D

Fig. 8 Key results of the hydraulic tests showing the permeability trends with fracture connections: Permeability associated with **a** The number and **b** Total length of intersection lines

5 Conclusion

The purpose of this study is to investigate the effects of fracture parameters on the absolute permeability of fractured rocks with extremely low matrix permeability by stochastic representation of natural fractures. Series of 3D stochastic fracture networks with different fracture length distribution, aperture and fracture number were established, and the effects of these fracture parameters on the micro-scale fluid flow were systematically investigated. The considered fractures are constituted of homogeneous isotropic convex polygons. The strike, dip angle and length value for each fracture were extracted from Uniform, Fisher and negative Exponential distributions, respectively. The flow velocity field was calculated using Finite-Difference method to solve Stokes equation. Then, the permeability of our rock samples was calculated using Darcy's law. We numerically acquired permeability of fractured rock samples. We compared the permeability corresponding to changes in the fracture number, aperture, and fracture length distribution of the fractures. From the numerical examples we come to some interesting conclusions.

1) We can see the importance of the fracture parameters to fluid flow in fractured rocks. It is the effective part of the fracture network that directly affects the permeability. The effective part of fracture network is determined by fracture number and the distribution of fracture length and aperture. We found that the fracture number and length variation increased the chances of fracture connection and tended to more fluid flow path, while the fracture aperture increase enhanced this fluid flow and tended to high permeability.

2) From different realization results of the same parameter combination, we found that high value parameters do result in more local distribution patterns of fractures, which can increase the complexity of the fluid flow and making relations between fracture parameters and permeability more complicated and uncertain.

3) The number and the total length of intersections of the fractures are almost linear with permeability. It is indicated that the connectivity features of fractures are a key factor affecting permeability.

These results could contribute to our understanding of the uncertain and nonlinear relationship between fracture parameters and permeability in the natural fractured rocks.

Data availability The data used to support the findings of this study are available from the corresponding author upon request.

Declarations

Conflict of Interest The authors declare no conflict of interest.

References

Amaziane B, Hontans T, Koebbe JV (2001) Equivalent permeability and simulation of two-phase flow in heterogeneous porous media. Comput Geosci 5:279–300. https://doi.org/10.1023/A:1014508622020

Cheng-Haw L, Chen-Chang L, Bih-Shan L (2006) The estimation of dispersion behavior in discrete fractured networks of andesite in Lan-Yu Island. Taiwan Environmental Geology 52:1297–1306. https://doi.org/10.1007/s00254-006-0568-7

de Dreuzy JR, Davy P, Bour O (2001a) Hydraulic properties of two-dimensional random fracture networks following a power law length distribution 1. Effective Connectivity Water Resour Res 37:2065–2078

de Dreuzy JR, Davy P, Bour O (2001b) Hydraulic properties of two-dimensional random fracture networks following a power law length distribution 2. Permeability of networks based on lognormal distribution of apertures. Water Resour Res 37:2079–2095. https://doi.org/10.1029/2001wr900010

Dong S, Zeng L, Dowd P, Xu C, Cao H (2018) A fast method for fracture intersection detection in discrete fracture networks. Comput Geotech 98:205–216. https://doi.org/10.1016/j.compgeo.2018.02.005

Fabricius IL, Baechle G, Eberli GP, Weger R (2007) Estimating permeability of carbonate rocks from porosity and vp /vs. Geophysics 72:E185–E191. https://doi.org/10.1190/1.2756081

Fadakar Alghalandis Y (2017) ADFNE: Open source software for discrete fracture network engineering, two and three dimensional applications. Comput Geosci 102:1–11. https://doi.org/10.1016/j.cageo.2017.02.002

Fang Y, Elsworth D, Cladouhos TT (2018) Reservoir permeability mapping using microearthquake data. Geothermics 72:83–100. https://doi.org/10.1016/j.geothermics.2017.10.019

Gerke KM et al (2018) Finite-difference method Stokes solver (FDMSS) for 3D pore geometries: Software development, validation and case studies. Comput Geosci 114:41–58. https://doi.org/10.1016/j.cageo.2018.01.005

Grana D, Caspari E, Holliger K, Quintal B (2014) Probabilistic approach to rock physics modeling. Geophysics 79:D123–D143. https://doi.org/10.1190/geo2013-0333.1

Hanano M (2004) Contribution of fractures to formation and production of geothermal resources. Renew Sustain Energy Rev 8:223–236. https://doi.org/10.1016/j.rser.2003.10.007

Huang N, Jiang Y, Liu R, Li B (2017) Estimation of permeability of 3-D discrete fracture networks: an alternative possibility based on trace map analysis. Eng Geol 226:12–19. https://doi.org/10.1016/j.enggeo.2017.05.005

Hunt AG (2005) Percolation theory and the future of hydrogeology. Hydrogeol J 13:202–205. https://doi.org/10.1007/s10040-004-0405-6

Khirevich S, Ginzburg I, Tallarek U (2015) Coarse- and fine-grid numerical behavior of MRT/TRT lattice-Boltzmann schemes in regular and random sphere packings. J Comput Phys 281:708–742. https://doi.org/10.1016/j.jcp.2014.10.038

Li B, Liu R, Jiang Y (2016) Influences of hydraulic gradient, surface roughness, intersecting angle, and scale effect on nonlinear flow behavior at single fracture intersections. J Hydrol 538:440–453. https://doi.org/10.1016/j.jhydrol.2016.04.053

Mostaghimi P, Blunt MJ, Bijeljic B (2013) Computations of absolute permeability on micro-CT images. Math Geosci 45:103–125. https://doi.org/10.1007/s11004-012-9431-4

Narsilio GA, Buzzi O, Fityus S, Yun TS, Smith DW (2009) Upscaling of Navier-Stokes equations in porous media: theoretical, numerical and experimental approach. Comput Geotech 36:1200–1206. https://doi.org/10.1016/j.compgeo.2009.05.006

Nathenson M (2000) The dependence of permeability on effective stress for an injection test in the Higashi-Hachimantai Geothermal Field. Geophys Res Lett 27:589–592. https://doi.org/10.1029/1999gl008394

Roy IG (2019) On studying flow through a fracture using self-potential anomaly: application to shallow aquifer recharge at Vilarelho da Raia, northern Portugal. Acta Geod Geophys 54:225–242. https://doi.org/10.1007/s40328-019-00256-6

Slatlem Vik H, Salimzadeh S, Nick HM (2018) Heat recovery from multiple-fracture enhanced geothermal systems: The effect of thermoelastic fracture interactions. Renewable Energy 121:606–622. https://doi.org/10.1016/j.renene.2018.01.039

Starnoni M, Pokrajac D, Neilson JE (2017) Computation of fluid flow and pore-space properties estimation on micro-CT images of rock samples. Comput Geosci 106:118–129. https://doi.org/10.1016/j.cageo.2017.06.009

Szabó NP, Kormos K, Dobróka M (2015) Evaluation of hydraulic conductivity in shallow groundwater formations: a comparative study of the Csókás' and Kozeny-Carman model. Acta Geod Geophys 50:461–477. https://doi.org/10.1007/s40328-015-0105-9

Tayari F, Blumsack S, Johns RT, Tham S, Ghosh S (2018) Techno-economic assessment of reservoir heterogeneity and permeability variation on economic value of enhanced oil recovery by gas and foam flooding. J Petrol Sci Eng 166:913–923. https://doi.org/10.1016/j.petrol.2018.03.053

Wang JA, Park HD (2002) Fluid permeability of sedimentary rocks in a complete stress–strain process. Eng Geol 63:291–300. https://doi.org/10.1016/s0013-7952(01)00088-6

Wei P, Pu W, Sun L, Pu Y, Wang S, Fang Z (2018) Oil recovery enhancement in low permeable and severe heterogeneous oil reservoirs via gas and foam flooding. J Petrol Sci Eng 163:340–348. https://doi.org/10.1016/j.petrol.2018.01.011

Xiong F, Jiang QH, Xu CS, Zhang XB, Zhang QH (2019) Influences of connectivity and conductivity on nonlinear flow behaviours through three-dimension discrete fracture networks. Comput Geotech 107:128–141. https://doi.org/10.1016/j.compgeo.2018.11.014

Xu P, Yu BM (2008) Developing a new form of permeability and Kozeny-Carman constant for homogeneous porous media by means of fractal geometry. Adv Water Resour 31:74–81. https://doi.org/10.1016/j.advwatres.2007.06.003

Zazoun RS (2008) The Fadnoun area, Tassili-n-Azdjer, Algeria: Fracture network geometry analysis. J Afr Earth Sc 50:273–285. https://doi.org/10.1016/j.jafrearsci.2007.10.001

Zhang Q-H, Yin J-M (2014) Solution of two key issues in arbitrary three-dimensional discrete fracture network flow models. J Hydrol 514:281–296. https://doi.org/10.1016/j.jhydrol.2014.04.027

Zhang Z, Nemcik J, Qiao Q, Geng X (2014) A model for water flow through rock fractures based on friction factor. Rock Mech Rock Eng 48:559–571. https://doi.org/10.1007/s00603-014-0562-4